S. GHOSH[1],✉

P. SRIVASTAVA[1]

B. PANDEY[1]

M. SAURAV[1]

P. BHARADWAJ[1]

D.K. AVASTHI[2]

D. KABIRAJ[2]

S.M. SHIVAPRASAD[3]

Study of ZnO and Ni-doped ZnO synthesized by atom beam sputtering technique

[1] Nanostech Laboratory, Department of Physics, Indian Institute of Technology Delhi, Hauz Khas, New Delhi 110016, India

[2] Inter University Accelerator Centre, Aruna Asaf Ali Marg, New Delhi 110067, India

[3] National Physical Laboratory, Dr. K.S. Krishnan Marg, New Delhi 110012, India

ABSTRACT Zinc oxide (ZnO) and Ni-doped zinc oxide (ZnO:Ni) films are prepared by atom beam sputtering with an intent of growing transparent conducting oxide (TCO) material and understanding its physical properties. The crystalline phases of the films are identified by the grazing angle X-ray diffraction (GAXRD) technique. Thicknesses of the films are measured by ellipsometry. Chemical states of the elements present in the films are investigated by X-ray photoelectron spectroscopy (XPS), which indicates the presence of Ni in the ZnO environment in a divalent state. Average transmission across the ZnO:Ni film was determined to be $\sim 83\%$ in the visible region, which is less than that ($\sim 90\%$) of undoped ZnO films. The resistivity measured by van der Pauw technique of the ZnO:Ni film ($\sim 9 \times 10^{-3}\ \Omega\,\mathrm{cm}$) is two orders of magnitude smaller as compared to its undoped counterpart ($1\ \Omega\,\mathrm{cm}$). For ZnO:Ni film an average carrier concentration of $\sim 1.4 \times 10^{19}\ \mathrm{cm}^{-3}$ was observed by Hall measurements. Two important mechanisms reported in the literature viz. influence of d–d transition bands and electron scattering from crystallites/grains are discussed as the possible causes for the increase in conductivity on Ni doping in ZnO.

PACS 73.50.Bk; 78.66.Li; 79.60.Dp; 61.05.cp

1 Introduction

Zinc oxide (ZnO), due to its specific electrical, optical and mechanical properties is one of the important wide band gap semiconductor materials. There is growing interest in ZnO due to its potential applicability in optoelectronic devices, such as light-emitting diodes, laser diodes and detectors for UV wavelength range. Properties of ZnO are very close to those of the widely recognized semiconductor, GaN. The band gap of ZnO (3.37 eV) is close to that of GaN (3.39 eV), but ZnO exciton binding energy (60 meV) is approximately two times larger than that of GaN (28 meV) [1], which makes it more promising as an optoelectronic material. The importance of metal-doped ZnO as TCO material has been discussed by different groups in the recent past [2–6]. Several reports on ZnO doped with Al, Ga, In, etc.

describing their optical, structural and electrical characteristics have been published recently [2–6]. It is also mentioned that doped ZnO can be prepared as a less expensive TCO material [7]. Important results of the above mentioned studies are: (i) Al-doped ZnO having transmittance $\sim 88\%$ and resistivity approximately $8.5 \times 10^{-5}\ \Omega\,\mathrm{cm}$ [5]; (ii) nanocrystalline ZnO:Ga films having resistivity $7 \times 10^{-4}\ \Omega\,\mathrm{cm}$ and average transparency $\sim 93\%$ [3]; (iii) synthesis of a p-type ZnO [4].

In earlier studies, doping of ZnO by transition metal elements was usually not tried, probably due to the incompatibility in the electron affinity or ionic radii of such elements with that of Zn. Of late, the motivation of making spintronic devices based on diluted magnetic semiconductors led the researchers to dope ZnO with Fe, Co, Ni, Mn etc. There are promising results in this area [8–10] and above room temperature ferromagnetism was realized in ZnO:Ni film recently [9, 10].

Doping of Ni in ZnO matrix has been done by several techniques [10–12], however, effect on resistivity of ZnO on Ni doping is not well established so far. Films grown by rf magnetron sputtering were found to be insulating up to a Ni concentration of 20% [11]. The Ni-doped (2 mol %) ZnO films prepared by spin coating showed a resistivity of $1.4 \times 10^{-1}\ \Omega\,\mathrm{cm}$ [13]. Singh et al. [14] have reported decrease in resistivity up to 2 mol % of Ni doping in bulk ZnO samples. Moreover, in a very recent communication, Wang et al. reported enhancement of resistivity in Ni-doped ZnO deposited by magnetron sputtering technique [12].

The present work is motivated to find a synthesis process for growing Ni-doped ZnO as transparent conducting oxide i.e., to enhance the electrical conductivity of the film, retaining of course optical transmission in the visible range to a high value. This kind of study may open up the possibility of synthesizing transition metal-doped transparent conducting oxide apart from their important usage as magnetic semiconductor material. Here we are reporting for the first time the synthesis of Ni-doped ZnO thin films grown by atom beam sputtering technique and a study of their transparent conducting properties.

2 Experimental details

A set of transparent films were grown on silicon and quartz substrates. For atom beam sputtering, an Ar atom gun source was mounted at 45° facing towards the sputter-

✉ Fax: +91-11-26581114, E-mail: ghoshsantanu1@yahoo.co.in

ing target (4 N ZnO disc of 2 inch diameter). The cleaned substrates were mounted at a variable gap below the target. The base pressure obtained in the chamber was 7×10^{-7} mbar with a turbo molecular-rotary pump combination. Deposition pressure was 2.6×10^{-3} mbar. The source delivered ~ 13 mA current on the target, with energy of ~ 1 keV. The area of the Ar beam was approximately 50 mm in diameter at the source. The ZnO disc is sputtered by Ar atom beam and ZnO films were deposited on the substrates. The time of deposition for both these films was 8 h. For deposition of ZnO:Ni films, Ni foils were glued to the ZnO disc and co-sputtered by the Ar beam. Crystalline phases of the films were identified by grazing angle X-ray diffraction technique with Cu K_α radiation in Bragg–Brantano geometry [15], and the crystallite size along z-direction was determined with the help of the Scherrer formula [16]. Thickness of the films deposited on Si substrate was determined to be 80 nm by ellipsometry. The presence of Ni was confirmed by X-ray fluorescence using a PHILIPS (MINIPAL) system. To identify the chemical states of the elements present in the film, X-ray photoelectron spectroscopy (XPS) measurements were carried out using Mg K_α radiation ($h\nu = 1253.3$ eV). The base pressure during the measurement was 5×10^{-10} Torr. The C $1s$ peak at 284.6 eV was used as a reference to take care of the shifts due to charging effect. All measurements were carried out at room temperature after sputtering the films for 3 min with Ar ions of 4 kV. The pressure during sputtering was 1×10^{-6} Torr. The resistivity and carrier concentration were measured in van der Pauw geometry. The measurements were carried out on a number of films deposited in the same batch and average values are reported in the next section. The optical transmittance measurement of these films was carried out with a HITACHI UV-VIS spectrometer.

3 Results and discussion

The calculation of film stoichiometry (Ni/ZnO) and results obtained from different characterization techniques are discussed in the following subsections.

3.1 Calculation of film stoichiometry

The film stoichiometry (Ni to ZnO ratio) was calculated by using the following expression:

$$\frac{\text{Ni}}{\text{ZnO}} = \frac{\left[\begin{array}{c}\text{effective area of Ni on ZnO target} \\ \times \text{sputtering yield of Ni at } 45°\end{array}\right]}{\left[\begin{array}{c}\text{effective area of ZnO target} \\ \times \text{sputtering yield of Ni at } 45°\end{array}\right]} \quad (1)$$

sputtering yield of ZnO at $45° = 6.6$ atoms/ion
sputtering yield of Ni at $45° = 4.2$ atoms/ion
diameter of ZnO target $= 50$ mm
dimension of one Ni foil $= (5 \times 5)$ mm^2
area of ZnO target $= \pi r^2$
$\qquad\qquad = 3.14 \times 25^2$
$\qquad\qquad = 3.14 \times 625 = 1962.5$ mm^2
area of Ni foils $= 4 \times 25$
$\qquad\qquad = 100$ mm^2
effective area of ZnO target $= (1962.5 - 100)$
$\qquad\qquad\qquad\qquad = 1862.5$ mm^2

$$\frac{\text{Ni}}{\text{ZnO}} = \frac{100 \times 4.2}{1862.5 \times 6.6} = 3.4\% . \quad (2)$$

3.2 Structural characterization

Typical GAXRD pattern of Ni-doped ZnO film is shown in Fig. 1. The pattern reveals that the film is polycrystalline in nature, having strongest peak corresponding to (002) plane at $2\theta = 33.72°$. These diffraction angles are smaller than in bulk ZnO, which can be explained on the basis of the work of Kuroyanagi et al. [17], who observed that the diffraction angle of the (002) for metal-doped ZnO shifts to lower angle due to ionization of ZnO. No metallic Zn or Ni characteristic peak is observed in the XRD study. Within the experimental error no new phase is observed in the ZnO:Ni film. In order to obtain crystallite size along z-direction the peak corresponding to 002 plane is fitted as shown in Fig. 2. The full width half maxima in ZnO film is $\sim 3°$ and that of ZnO:Ni film is $\sim 1°$.
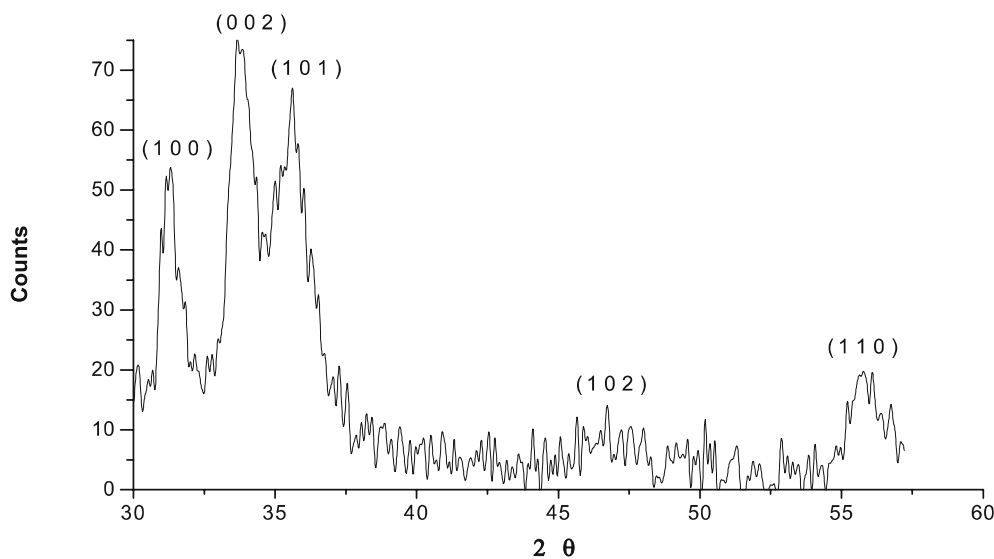

FIGURE 1 A typical glancing angle X-ray diffraction pattern of ZnO:Ni/ quartz film. Similar spectrum was obtained for the film deposited on silicon substrate
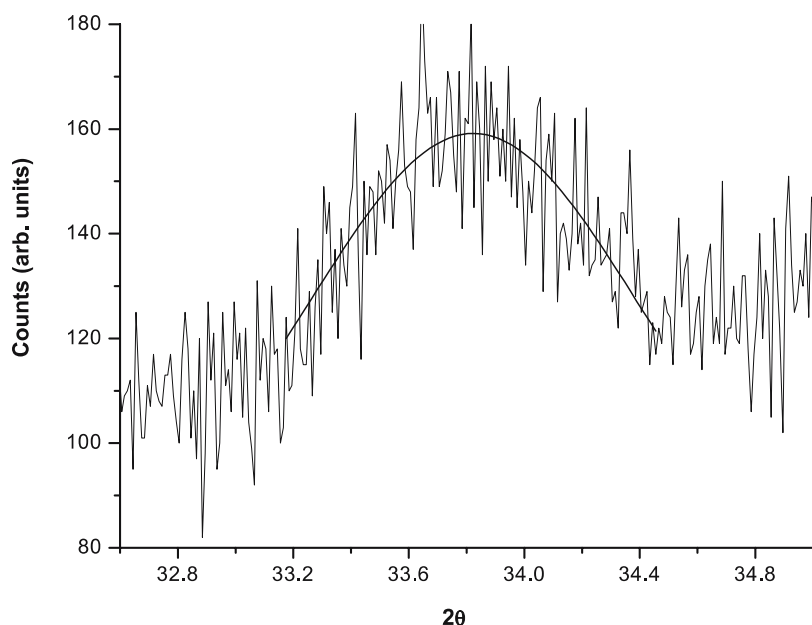
FIGURE 2   Gaussian fit of the peak corresponding to 002 plane of ZnO:Ni/quartz film is shown for the determination of crystallite size
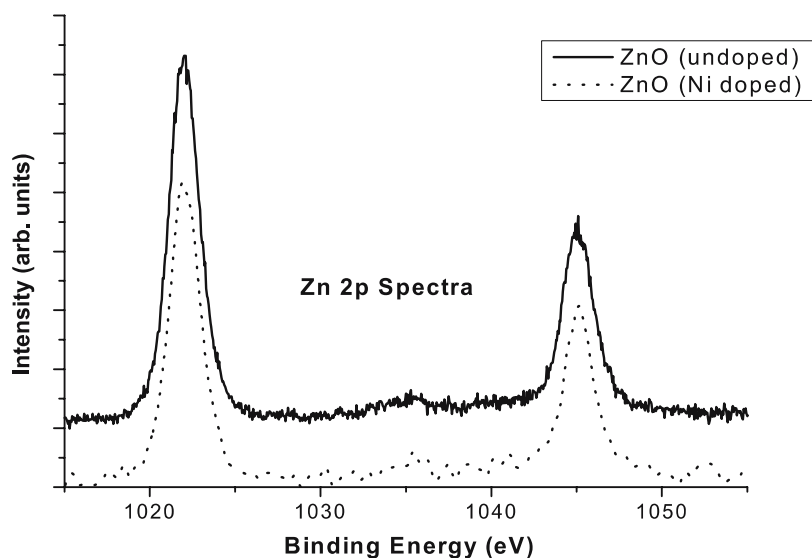

FIGURE 3   Zn $2p$ core level XPS spectra of pure and Ni-doped ZnO film. No changes were observed in the spectrum on Ni doping

With the help of the Scherrer formula, the average crystallite size is found to be ~ 3 nm and ~ 10 nm for pure and Ni-doped ZnO films, respectively.

3.3   *XPS measurements*

The chemical states of the elements present are discussed on the basis of XPS measurement. Figure 3 shows Zn $2p$ spectra of both the films. The spectrum does not show any significant change on Ni doping. Figure 4 shows Ni $2p_{3/2}$ peak of the Ni-doped ZnO film. It shows a clear satellite structure around 860 eV. Similar satellite peaks were observed for nickel oxides previously and is ascribed to $O(2p) \rightarrow Ni(3d)$ charge-transfer transition or hybridization [18, 19]. The presence of the satellite peak in Ni-doped ZnO films indicates that nickel is present in an oxygen environment in the film. Ni may be incorporated in the ZnO crystallite as interstitial or substitutional impurities. However, the binding energy pos-

ition (~ 854 eV) of Ni $2p_{3/2}$ is quite close to the one reported for NiO [20]. Therefore, present XPS measurements strongly suggest that in the doped films Ni^{2+} ions partly substitute Zn in the ZnO matrix and rule out the presence of Ni in metallic or +3 states.

3.4   *Optical characterization*

Figure 5 shows transmittance versus wavelength curves for both pure and Ni-doped ZnO films. These measurements were carried out on the films, which were deposited on quartz substrates. The figure shows that in the wavelength range between 400–800 nm, the pure ZnO film has a transmission of $\sim 90\%$. Though, doping of Ni slightly reduces the transmission, there is not much change ($\sim 7\%$) in maximum transmission value. A small blue shift is observed suggesting an increase in band gap values on doping. The observed results in enhancement of band gap can be attributed to the
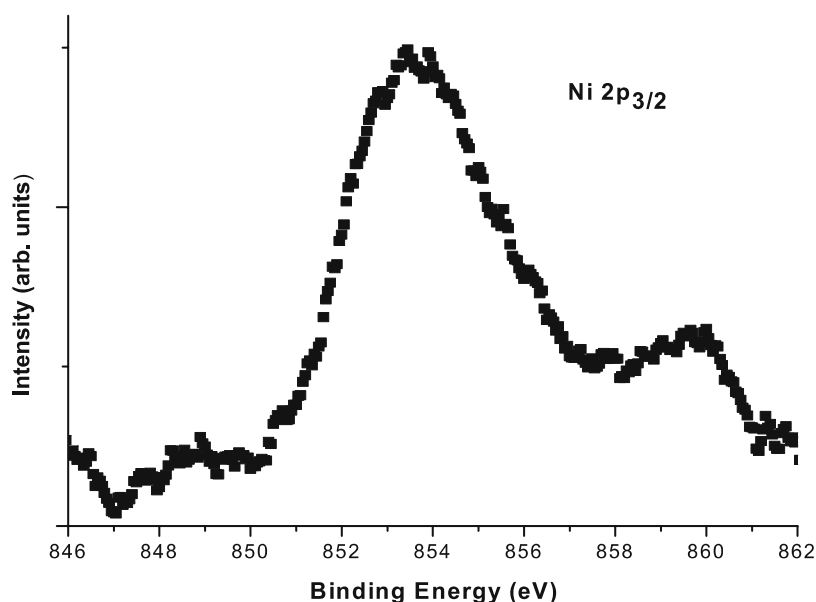
FIGURE 4 Ni $2p_{3/2}$ core level XPS spectrum of Ni-doped ZnO film. A satellite structure close to 860 eV can be seen clearly
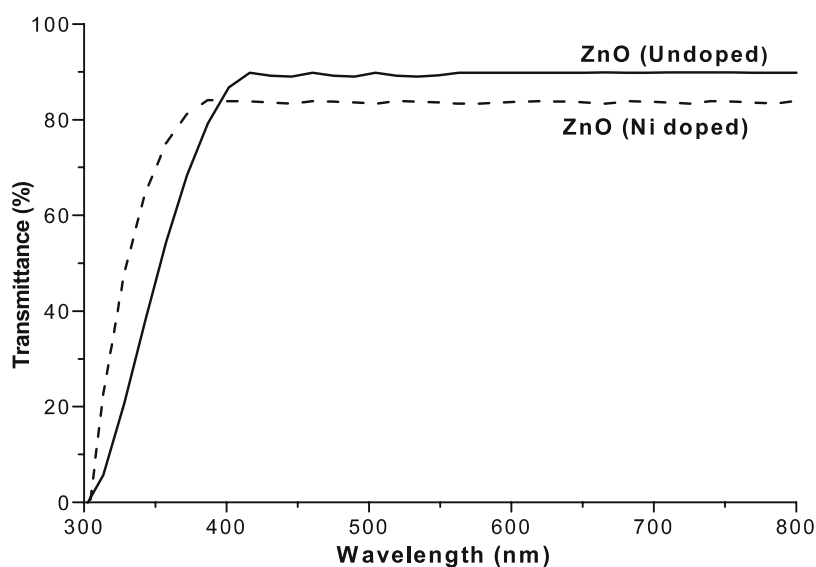

FIGURE 5 Transmittance versus wavelength of ZnO/quartz and ZnO:Ni/quartz films. A small blue shift is observed on Ni doping

Burstein–Moss effect [2, 21]. We will come back to this point while discussing the conduction mechanism.

3.5   *Transport properties*

The resistivity measurement shows a significant decrease (more than two orders) of the resistivity value in ZnO:Ni as compared to undoped ZnO film. The pure ZnO has a resistivity of $\sim 1\,\Omega\,cm$ whereas for the Ni-doped film the value is $9 \times 10^{-3}\,\Omega\,cm$. To have a better understanding of the decrease in resistivity, Hall measurements were carried out at room temperature. The carrier concentration in the Ni-doped ZnO film was found to be $1.4 \times 10^{19}\,cm^{-3}$, which is in fair agreement with the reported one [8]. The film shows n-type conduction.

The reason for the decrease in resistivity on Ni doping is not very well understood. However, the present XPS measurements rule out the presence of Ni^{3+}, cited as the reason for decrease in resistivity at low doping concentrations [8].

Also, no indication of metallic Ni was found that may decrease resistivity.

The *ab initio* electronic structure calculations report existence of half metallic behavior in V, Cr, Fe, Co and Ni-doped ZnO [20]. The electronic band calculations carried out within the frame work of local density approximation (LDA) suggest the E_F's of ZnO:Fe, Co, Ni are located near the top of the valence band and partial density of states (PDOS) values of Fe, Co and Ni at E_F are relatively large [21]. As pointed out by Singh et al. [14], the Ni d-states appearing near the E_F may be split into e_g and t_{2g} states under the influence of tetrahedral crystal field of ZnO. The t_{2g} state on hybridization with p orbitals of the valence band further splits into bonding and anti-bonding states. The anti-bonding states having higher energies and itinerant electrons lie very close to the bottom of the conduction band (CB). The presence of itinerant electrons gives rise to increase in conductivity. In our case, these anti-bonding states seem to have merged with the CB as we observe not only an increase in electrical conductivity

on Ni doping but also a slight increase in optical band gap. However, since the DOS close to the E_F are also quite sensitive to oxygen derived states, a detailed and careful study such as valence band photoemission is required on these films to substantiate/refute aforementioned arguments.

Other mechanism that can affect electron transport in the polycrystalline TCO films is scattering from crystallites or grains [3]. Grain boundaries, across which crystal orientations change, are expected to be effective electron scatterer and behave like film interfaces. For smaller crystallite size contribution to film resistivity from this scattering is large. In the present case as the crystallite size is larger in ZnO:Ni film as compared to ZnO film and hence the probability of this scattering is less than in the former leading to a decrease in resistivity value.

As mentioned earlier, further studies are required to completely understand the conduction mechanism of ZnO and ZnO:Ni films deposited by atom beam sputtering, a technique, reported for the first time to grow ZnO based TCO film.

4   Conclusion

Polycrystalline ZnO and ZnO:Ni films of thickness ~ 80 nm are deposited by atom beam sputtering. Crystalline phases of the films and crystallite size are determined by grazing angle X-ray diffraction. The present results reveal incorporation of Ni in the ZnO matrix, most probably at the Zn sites in a $+2$ state. The resistivity of the ZnO:Ni film ($\sim 9 \times 10^{-3}$ Ω cm) is found to be two orders of magnitude smaller as compared to pure ZnO film (1 Ω cm). Two important mechanisms reported in the literature viz. influence of d–d transition bands and electron scattering from crystallites/grains are discussed as the possible causes for the increase in conductivity on Ni doping in ZnO. The reduction in resistivity in the Ni-doped ZnO film and an average transmission across the visible spectrum of $\sim 83\%$ qualify this system to be an important candidate for TCO material.

REFERENCES

1 C. Chen, F. Jen, Y.C. Lu, H.C. Wang, C.C. Yang, B.P. Zhang, Y. Segawa, Symp. N, ICMAT-2005, Singapore, July (2005)

2 S.H. Jeong, J.W. Lee, S.B. Lee, J.H. Boo, Thin Solid Films **435**, 78 (2003)

3 J.J. Robbins, J. Harvey, J. Leaf, C. Fry, C.A. Wolden, Thin Solid Films **473**, 35 (2005)

4 N. Sanmyo, Y. Tomita, K. Kobayashi, Key Eng. Mater. **248**, 87 (2003)

5 H. Agura, A. Suzuki, T. Matsushita, T. Aoki, M. Okuda, Thin Solid Films **445**, 263 (2003)

6 T. Minami, Semicond. Sci. Technol. **20**, S35 (2005)

7 Z.-Z. Ye, J.-F. Tang, Appl. Opt. **28**, 2817 (1989)

8 T. Wakano, N. Fujimura, Y. Morinaga, N. Abe, A. Ashida, T. Ito, Physica E **10**, 260 (2001)

9 D.A. Schwartz, K.R. Kittilstved, D.R. Gamelin, Appl. Phys. Lett. **85**, 1395 (2004)

10 P.V. Radovanovic, D.R. Gamelin, Phys. Rev. Lett. **91**, 157202 (2003)

11 Z. Yin, N. Chen, F. Yang, S. Song, C. Chai, J. Zhong, H. Qian, K. Ibrahim, Solid Stat. Commun. **135**, 430 (2005)

12 X.B. Wang, C. Song, D.M. Li, K.W. Geng, F. Zeng, F. Pan, Appl. Surf. Sci. **253**, 1639 (2006)

13 D. Shimono, S. Tanaka, T. Torikai, T. Watari, M. Murano, J. Ceram. Proc. Res. **2**, 184 (2001)

14 S. Singh, N. Rama, M.S. Ramachandra Rao, Appl. Phys. Lett. **88**, 222111 (2006)

15 B.D. Culity, *Elements of X-ray Diffraction* (Addison-Wesley, Reading, MA, 1978), p. 102

16 B.D. Cullity, S.R. Stock, *Elements of X-ray Diffraction* (Prentice Hall, Englewood Cliffs, NJ, 2001), p. 194

17 A. Kuroyanagi, J. Appl. Phys. **66**, 5492 (1989)

18 K.S. Kim, R.E. Davis, J. Electron. Spetrosc. Relat. Phenom. **1**, 251 (1972/1973)

19 S. Hüfner, G.K. Wertheim, Phys. Rev. B **8**, 4857 (1973)

20 G.H. Yu, L.R. Zeng, F.W. Zhu, C.L. Chai, W.Y. Lai, J. Appl. Phys. **90**, 4039 (2001)

21 E. Burstein, Phys. Rev. **93**, 632 (1954)

22 H. Katayama-Yoshida, K. Sato, Physica B **327**, 337 (2003)

23 Y. Imai, A. Watanabe, J. Mater. Sci. Mater. Electron. **15**, 743 (2004)